

Exchange-renormalized crystal field excitations in the quantum Ising magnet KTmSe_2 Shiyi Zheng ^{1,2,*}, Hongliang Wo ^{1,2,*}, Yiqing Gu ^{1,2,*}, Rui Leonard Luo ³, Yimeng Gu ^{1,2}, Yinghao Zhu ¹, Paul Steffens,⁴ Martin Boehm,⁴ Qisi Wang ^{1,5}, Gang Chen ^{6,3,†} and Jun Zhao ^{1,2,7,8,‡}¹State Key Laboratory of Surface Physics and Department of Physics, Fudan University, Shanghai 200433, China²Shanghai Qi Zhi Institute, Shanghai 200232, China³Department of Physics and HKU-UCAS Joint Institute for Theoretical and Computational Physics at Hong Kong, The University of Hong Kong, Hong Kong, China⁴Institut Laue-Langevin, 71 Avenue des Martyrs, 38042 Grenoble Cedex 9, France⁵Department of Physics, The Chinese University of Hong Kong, Shatin, Hong Kong, China⁶International Center for Quantum Materials, School of Physics, Peking University, Beijing 100871, China⁷Institute of Nanoelectronics and Quantum Computing, Fudan University, Shanghai 200433, China⁸Shanghai Research Center for Quantum Sciences, Shanghai 201315, China

(Received 22 May 2023; revised 1 August 2023; accepted 7 August 2023; published 23 August 2023)

Rare-earth delafossite compounds, ARC_2 (A = alkali or monovalent ion, R = rareearth, C = chalcogen), have been proposed for a range of novel quantum phenomena. Particularly, the Tm series, ATmC_2 , featuring Tm ions on a triangular lattice, serves as a representative group of compounds to illustrate the interplay and competition between spin-orbit coupling, crystal fields, and exchange couplings in the presence of geometric frustration. Here we report the thermodynamic and inelastic neutron scattering studies on the newly discovered triangular-lattice magnet KTmSe_2 . Both heat capacity and neutron diffraction measurements reveal the absence of long-range magnetic order. Magnetic susceptibility shows strong Ising-like interactions with antiferromagnetic correlations. Furthermore, inelastic neutron scattering measurements reveal a branch of dispersive crystal field excitations. To analyze these observations, we employ both the transverse field Ising model and the full crystal field scheme, along with exchange interactions. Our results suggest a strong competition between spin exchange interactions and crystal field effects. This work is expected to offer a valuable framework for understanding low-temperature magnetism in KTmSe_2 and similar materials.

DOI: [10.1103/PhysRevB.108.054435](https://doi.org/10.1103/PhysRevB.108.054435)**I. INTRODUCTION**

Recent theoretical and experimental studies on the triangular-lattice magnets with strong frustration and quantum fluctuation have proposed several possible realizations of exotic quantum states [1,2]. Two common scenarios, involving triangular lattices occupied by either Kramers or non-Kramers ions, have been extensively investigated to elucidate unconventional magnetic ground states. A well-known example of the former case is the quantum spin liquid (QSL) material YbMgGaO_4 [3–11], while TmMgGaO_4 with the integer spin local moments could be approximately viewed as an example of the non-Kramers doublets [12–16]. Despite the successful description of the transverse field Ising model (TFIM) [13,14,17,18] in TmMgGaO_4 , further examination and research are necessary to address fundamental questions regarding the nature of magnetic excitations in generic non-Kramers triangular-lattice magnets.

Since crystal electric field (CEF) interactions play a vital role in determining both the magnetic ground state and

single-ion anisotropy of rare-earth ions [19–21], it is essential to uncover the CEF spectra in order to understand the exotic quantum states found in triangular-lattice magnets. In addition to determining the CEF parameters and eigenvalues, measuring the dispersion or splitting of the low-lying CEF states may also provide useful information about low-temperature magnetism, including dipole-dipole interactions [22], phonon modes [23–25], and quadrupolar excitons [26,27].

In the last few years, a new class of triangular-lattice antiferromagnets, ARC_2 (A = alkali or monovalent ion, R = rareearth, C = chalcogen), has attracted great attention due to its potential in realizing novel quantum states [28]. This family of materials crystallizes into a delafossite structure with space group $R\bar{3}m$ or $P6_3/mmc$, while the trivalent R^{3+} ions reside in a local environment with D_{3d} symmetry. Tremendous investigations on Yb^{3+} - [29–38], Er^{3+} - [39–41], and Ce^{3+} -based [42–44] 112-family magnets have been reported, including massive precise knowledge of the CEF excitations in them [45–52]. However, while the majority of studies focus on materials in which the triangular lattice is formed by Kramers ions in the ARC_2 family, research on compounds featuring non-Kramers ions is rather limited. Unraveling the magnetic properties of these compounds remains an important task. KTmSe_2 , the new thulium-based 112-family material, shares the same crystal structure as

*These authors contributed equally to this work.

†gangchen@hku.hk

‡zhaoj@fudan.edu.cn

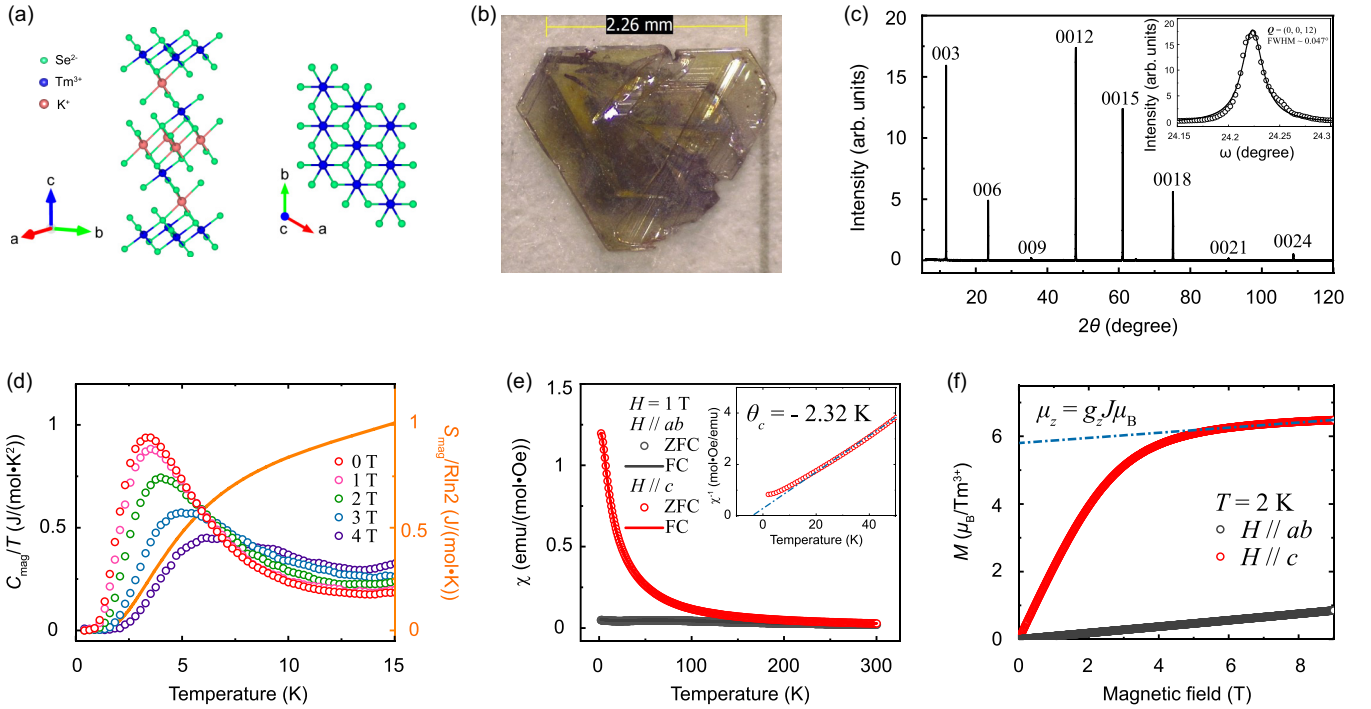


FIG. 1. (a) Schematic of the crystal structure of KTmSe_2 . Blue, Tm^{3+} ; red, K^+ ; green, Se^{2-} . (b) Image of a typical single crystal. (c) X-ray diffraction pattern of KTmSe_2 single crystal on the $(0, 0, L)$ plane. (d) Heat capacity and entropy release of KTmSe_2 under different magnetic fields along the c axis. (e) Temperature dependence of magnetic susceptibility from 2 to 300 K for KTmSe_2 single crystal both in the ab plane and along the c axis under 1 T. The inset shows the inverse magnetic susceptibility with negative Curie-Weiss temperature. (f) Isothermal magnetization of KTmSe_2 up to 9 T both in the ab plane and along the c axis at 2 K. FWHM, full width at half maximum; FC, field cooled; ZFC, zero-field cooled.

the QSL materials NaYbO_2 [29] and NaYbSe_2 [35]. The perfect triangular-lattice layers of magnetic Tm^{3+} ions are separated by the nonmagnetic K^+ layers, resulting in a quasi-two-dimensional structure with geometrical frustration [see Fig. 1(a)]. The two lowest CEF levels of the non-Kramers Tm^{3+} ion are point-group-symmetry-demanded singlets. Nevertheless, the first excited CEF state is highly dispersive in the reciprocal space, and this is attributed to the strong renormalization of the CEF excitation by the exchange interactions of the local moments. The quantitative measurement of these excitations provides a great chance to determine the exchange parameters and the CEF energy levels.

In this paper, we report the thermodynamic and neutron scattering measurements and point-charge calculations on the single-crystalline triangular-lattice magnet KTmSe_2 to investigate the competition between the exchange coupling and the CEF effect by directly revealing the exchange-renormalized CEF excitations. Heat capacity and neutron diffraction measurements show the absence of long-range magnetic order in KTmSe_2 down to an ultralow temperature of 60 mK. The temperature-dependent susceptibility and the field-dependent magnetization show the Ising-like single-ion anisotropy and predominantly antiferromagnetic spin correlations accompanied by a negative Curie-Weiss (CW) temperature. Inelastic neutron scattering (INS) illustrates a branch of dispersive excitation from 0.85 to 1.6 meV which is the first excited CEF state of Tm^{3+} , indicating that a single-ion model can no longer describe the low-lying CEF excitations. A frequently used solution is to apply the transverse field Ising model

(TFIM) on KTmSe_2 to explain the dispersive magnetic excitation by constructing a pseudospin $S_{\text{eff}} = 1/2$ from the ground state quasideublet [12,13,16–18]. The effective model successfully explains the dispersive magnetic excitation by introducing a transverse field perpendicular to the z axis, and provides a phase diagram that can include many different materials with similar Ising characters. From a more complete perspective, establishing an effective magnetic Hamiltonian consisting of all the CEF states and the spin exchange parameters simultaneously is also productive and illustrative. As a complementary approach to the TFIM, we then apply point-charge (PC) analysis and the mean-field-random-phase approximation (MF-RPA) to calculate the CEF spectra and low-energy magnetic excitations.

The remaining parts of the paper are organized as follows. In Sec. II, we introduce the experimental details. In Sec. III, we propose a TFIM for the low-lying doublets with the effective spin S_{eff} to account for the dispersive CEF excitation. In Sec. IV, we include all the CEF states and the superexchange with the local J moments to further analyze the CEF excitations. In Sec. V, we conclude with a discussion.

II. EXPERIMENTAL METHOD AND RESULTS

Polycrystalline samples of KTmSe_2 were synthesized through a solid-state reaction with a molar ratio of $\text{K} : \text{Tm} : \text{Se} = 1 : 1 : 2$. The starting materials were sealed in a vacuumed quartz tube and heated to 950 °C at a rate of

TABLE I. Refined crystallographic parameters for KTmSe_2 polycrystal (trigonal, space group $R\bar{3}m$, $Z = 3$) from room-temperature x-ray powder diffraction with pulverized single-crystal KTmSe_2 samples.

Lattice parameter	Value
a (Å)	4.1352(1)
c (Å)	22.7487(5)
V (Å ³)	336.881(2)
α (deg)	90
γ (deg)	120
Atomic position	Value
	K
(x, y, z)	(0, 0, 0.5)
Wyckoff site	b
Multiplicity	3
	Tm
(x, y, z)	(0, 0, 0)
Wyckoff site	a
Multiplicity	3
	Se
(x, y, z)	[0, 0, 0.2698(1)]
Wyckoff site	c
Multiplicity	6

50 °C/h and then maintained at this temperature for 3 days. KTmSe_2 single crystals were grown by the flux method with a molar ratio of $\text{KTmSe}_2 : \text{K}_2\text{Se}_3 = 1 : 10$. The powder mixture was annealed at 950 °C for 5 h and then slowly cooled down to 650 °C at a rate of 0.8 °C/h. The flux was subsequently removed with deionized water. KLuSe_2 single crystals, used as a nonmagnetic reference, were grown using the same method. The resulting dark yellow KTmSe_2 single crystal exhibited a hexagonal shape with well-defined edges [Fig. 1(b)]. Single-crystal x-ray diffraction measurements were performed on a Bruker D8 x-ray diffractometer [Fig. 1(c)]. The x-ray powder diffraction data were refined using the FULLPROF SUITE software [53], from which the crystallographic parameters were extracted. A summary of the relevant crystallographic parameters for the KTmSe_2 is provided in Table I.

Heat capacity, susceptibility, and magnetization measurements on KTmSe_2 single crystals were performed on a PPMS DynaCool instrument (Quantum Design). No signal of magnetic phase transition is observed in the heat capacity data under zero or nonzero external field along the crystalline c axis, indicating the absence of long-range magnetic order in KTmSe_2 compound down to at least 0.3 K [Fig. 1(d)]. A broad peak appears at ~ 4 K and can be then partially suppressed by external magnetic fields, implying a large contribution from excited CEF states. The temperature-dependent susceptibility shows Ising-like single-ion magnetic anisotropy with an evident easy axis and a negligible in-plane response. Moreover, the predominantly antiferromagnetic correlations are evidenced by the negative CW temperature of $\theta_c = -2.32$ K (fit from 20 to 50 K after subtracting the Van Vleck contribution) [Fig. 1(e)]. The isothermal magnetization data in both directions at 2 K reaffirm the Ising anisotropy, indicating that only the out-of-plane component requires examination

[Fig. 1(f)]. Upon reaching 6 T, the magnetization saturates and increases linearly with the applied field. The saturated magnetic moment is $\mu_z = 6.2 \mu_B$, from which we extract the g factor $g_z = 1.033$ ($\mu_z = g_z J \mu_B = 6g_z \mu_B$). The g factor is close to the Landé g factor of the Tm^{3+} ion $g_J = 1.167$, further confirming the Ising nature of KTmSe_2 . Inelastic neutron scattering data were collected on 3 g of KTmSe_2 single crystals in the $(H, K, 0)$ scattering plane. The measurements were carried out on the ThALES cold triple-axis spectrometer using a flat-cone analyzer at the Institut Laue-Langevin, Grenoble, France.

No magnetic Bragg peak is observed at high-symmetry points down to 60 mK in neutron diffraction measurements, confirming the absence of long-range magnetic order in KTmSe_2 , as indicated by the heat capacity data. With the increase in energy, a branch of dispersive magnetic excitation becomes visible at the K point [Fig. 2(a)]. The excitation disperses outward from the K point [Fig. 2(b)] and then forms ringlike patterns around the Γ point at higher energies [Figs. 2(c)–2(e)]. Eventually, the spectra reach the band top at the Γ point and vanish above 1.6 meV [Fig. 2(f)]. The overall dispersion is seen more clearly in the energy dependence of the spectral intensity along the high-symmetry directions [Fig. 3(a)] and in a group of constant-energy cuts [Fig. 4(a)]. Based on constant- Q cuts at the high-symmetry points, we can quantitatively determine a spin gap of 0.887 ± 0.066 meV (at the K point) in KTmSe_2 [Fig. 4(b)], while the total bandwidth of the magnetic excitation is 0.649 ± 0.144 meV [Fig. 4(d)]. To describe the observed magnetic excitation spectrum, we need to carry out the theoretical process.

III. QUANTUM ISING MODEL DESCRIPTION WITH LOWER DOUBLETS

An effective spin-1/2 model is widely used to treat the low-energy magnetic excitations in many rare-earth magnets, assuming that the magnetic properties at low temperatures are governed by the interaction between the $S_{\text{eff}} = 1/2$ local moments with no involvement of higher excited CEF states. In the triangular-lattice compound TmMgGaO_4 , a quasidoublet consisting of the two lowest singlets with an energy gap of ~ 0.62 meV is considered as the magnetic ground state, corresponding to a pseudospin-1/2 with an effective transverse field along the y direction [13,18]. In this picture, the out-of-plane spin operator \hat{S}^z represents the three-sublattice dipole, order while the in-plane operators \hat{S}^x and \hat{S}^y represent the ferroquadrupole order, described with transverse field Ising model [17,18]. We here apply the same quantum Ising model description to explain the dispersive magnetic excitation in KTmSe_2 observed in INS. Unlike TmMgGaO_4 , where the exchange interaction wins and supports an ordered state via the assistance of the intrinsic transverse Zeeman coupling by an order-by-disorder mechanism [13,18], the intrinsic transverse Zeeman coupling wins and preserves the \mathbb{Z}_2 symmetry of the system in KTmSe_2 .

In the magnetization measurements on single-crystalline samples, the Tm^{3+} ions are fully polarized under large magnetic fields (upon 8 T), from which we find that the g factor $g_z = 1.033$ is close to the Landé factor $g_J = 1.167$. The single-ion Ising anisotropy suggests that the ground state wave

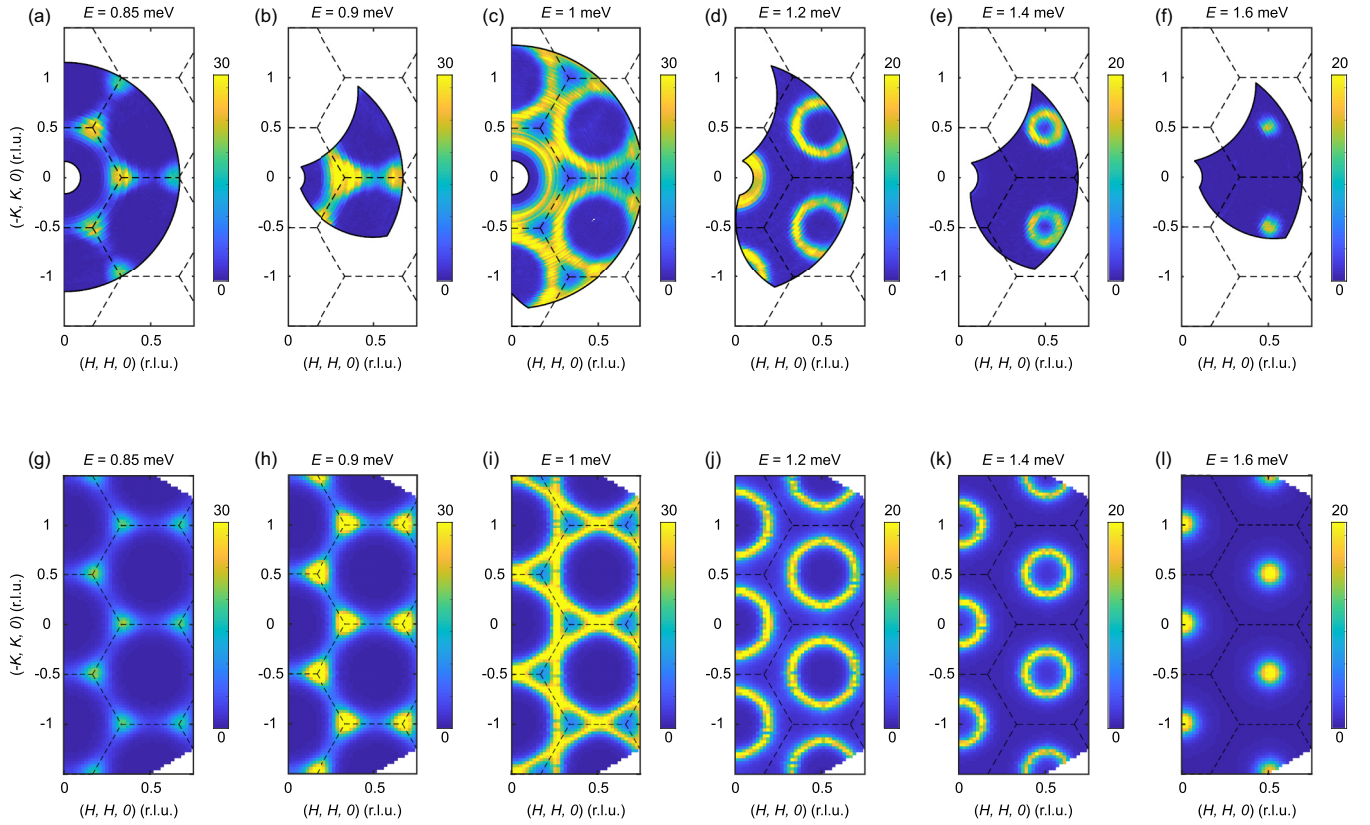


FIG. 2. Measured and calculated momentum dependence of the CEF excitation in KTmSe₂ at the indicated energies and $T = 0.06$ K. (a)–(f) Raw contour plots of the constant-energy images at $T = 0.06$ K. (g)–(l) Calculated CEF excitation using the MF-RPA model specified in the text. The dashed lines indicate the zone boundaries. The measurements were performed on ThALES triple-axis spectrometer with $E_f = 4.066$ meV. Here, r.l.u., reciprocal lattice units.

function of KTmSe₂ is dominated by $|J^z = \pm 6\rangle$, which means that the CEF ground state is a singlet [14],

$$|\Psi_g\rangle = c_6(|6\rangle + |-6\rangle) + c_3(|3\rangle - |-3\rangle) + c_0|0\rangle; \quad (1)$$

additionally, in our heat capacity measurements, the full magnetic entropy release shows $\sim R \ln 2$ around 15 K, indicating that the first excited CEF state is supposed to be another singlet,

$$|\Psi_e\rangle = c'_6(|6\rangle - |-6\rangle) + c'_3(|3\rangle + |-3\rangle). \quad (2)$$

The CEF information obtained from characterizations suggests that the ground state of KTmSe₂ is expected to be a “quasidoublet,” consisting of the CEF ground state singlet and the first excited singlet [13], similar to the case of TmMgGaO₄. As a result, we can construct effective spin-1/2 operators acting on this quasidoublet.

$$\hat{S}^x = \frac{i}{2}(|\Psi_e\rangle\langle\Psi_g| - |\Psi_g\rangle\langle\Psi_e|), \quad (3)$$

$$\hat{S}^y = \frac{1}{2}(|\Psi_g\rangle\langle\Psi_g| - |\Psi_e\rangle\langle\Psi_e|), \quad (4)$$

$$\hat{S}^z = \frac{1}{2}(|\Psi_g\rangle\langle\Psi_e| + |\Psi_e\rangle\langle\Psi_g|), \quad (5)$$

where $|\Psi_g\rangle$ and $|\Psi_e\rangle$ are eigenstates corresponding to eigenvalues of $1/2$ and $-1/2$ of \hat{S}^y . It has to be emphasized that the definition of the spin operators in Eqs. (3)–(5)

is to some extent different from the conventional meaning. The constructed longitudinal component \hat{S}^z behaves as a magnetic dipole which couples to neutron or external fields, while the transverse components \hat{S}^x and \hat{S}^y are even under time reversal and represent the multipolar behaviors displaying “hidden” in conventional experimental probes [13,18].

Based on the spin operators of the quasidoublet, we further establish the spin Hamiltonian of KTmSe₂ and adopt the linear spin wave (LSW) theory to calculate the spin excitation spectra,

$$\hat{H} = \sum_{\langle i,j \rangle} J_1 \hat{S}_i^z \hat{S}_j^z + \sum_{\langle\langle i,j \rangle\rangle} J_2 \hat{S}_i^z \hat{S}_j^z - h \sum_i \hat{S}_i^y, \quad (6)$$

where $\langle i,j \rangle$ and $\langle\langle i,j \rangle\rangle$ denote the nearest and next-nearest neighbors, respectively, and h is the energy corresponding to the effective intrinsic transverse field describing the splitting of the ground state quasidoublet, as described with TFIM [12,13,16–18]. A set of parameters can describe the neutron scattering data accurately: $J_1 = 0.29(1)$ meV, $J_2 = 0.018(2)$ meV, and $h = 1.13(2)$ meV. The calculated results reasonably agree with the experimental observations [Fig. 3(b)].

The successful application of the quantum Ising spin model both in TmMgGaO₄ [13,18] and in KTmSe₂ provides a unique method to understand the magnetic excitation in Ising

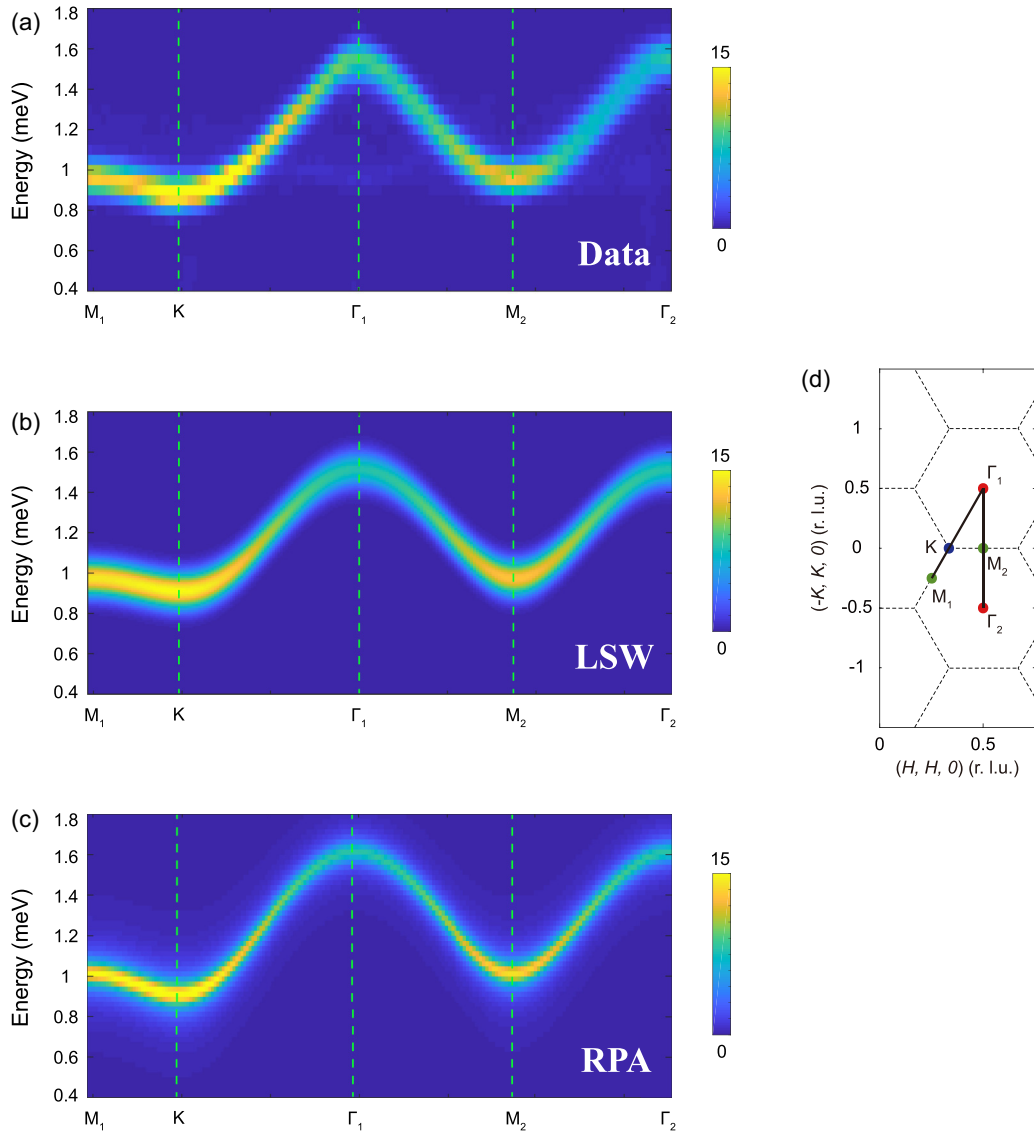


FIG. 3. (a) Energy dependence of the observed spectral intensity along the high-symmetry momentum direction at $T = 0.06$ K. (b) and (c) Simulated magnetic excitation spectra based on LSW and MF-RPA methods, respectively. (d) Schematic of a high-symmetry direction of KTmSe_2 .

antiferromagnets by introducing an effective transverse field to describe the splitting of the ground state quasidoublet. Comparing these two materials, we found that TmMgGaO_4 is located in the three-sublattice ordered state while KTmSe_2 is in the quantum disordered state that is driven by the dominant transverse exchange. These results are consistent with the general phase diagram tackled with the Weiss mean-field approximation [18]. Quite remarkably, the simple TFIM provides us with a unified understanding of these two compounds: Since the quantum order-by-disorder effect in TmMgGaO_4 is relatively weak, a coexistence of three-sublattice magnetic order and “ferroquadrupole hidden order” displays as a nearly gapless magnetic excitation in INS, while a relatively large effective transverse field h in KTmSe_2 results in the dominance of the polarization effect and suppression of the three-sublattice order and then drives the system into the “quantum disordered” state where the effective spins are fully polarized along the transverse direction.

IV. FULL CRYSTAL FIELD SCHEME CALCULATION

In the phase diagram of the TFIM, KTmSe_2 is located in the fully polarized region where the three-sublattice ordering is fully suppressed by the intrinsic polarization effect. This is consistent with the results from the heat capacity and neutron diffraction measurements. Due to the absence of long-range spin order, the dispersive excitation observed in the INS can also be considered as the first excited CEF state from another perspective. On the other hand, the spin exchange interaction between Tm^{3+} ions still plays an important role and is responsible for the dispersion for CEF excitations.

By establishing a CEF Hamiltonian below, we can then describe the CEF states of Tm^{3+} quantitatively,

$$\hat{H}_{\text{CEF}} = \sum_{n,m} B_n^m \hat{O}_n^m, \quad (7)$$

where \hat{O}_n^m are the Stevens operators and B_n^m are multiplicative factors called the CEF parameters [54]. Under the D_{3d} point

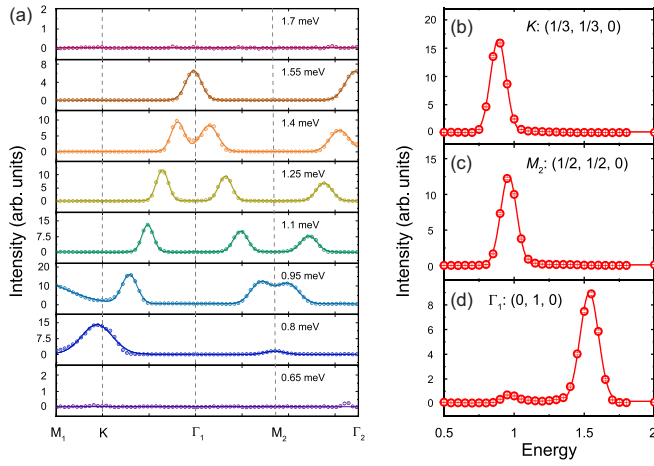


FIG. 4. (a) Constant-energy cuts along the M_1 - K - Γ_1 - M_2 - Γ_2 direction at the indicated energies at $T = 0.06$ K. The vertical dashed lines indicate the high-symmetry points. (b)–(d) Constant- Q cuts at the K , M , and Γ points, determining the spin gap and bandwidth of magnetic excitation in KTmSe_2 . The solid lines and error bars denote the Gaussian fits and standard deviation.

symmetry, only six CEF parameters are allowed to be nonzero in Eq. (7): B_2^0 , B_4^0 , B_4^3 , B_6^0 , B_6^3 , and B_6^6 . The 13-fold ($J = 6$, $L = 5$, $S = 1$) degenerate ground state of the free $4f^{12}$ Tm^{3+} is split into five singlets and four doublets under the D_{3d} CEF environment with a rotation axis about c [14]. We have used the MCPHASE software package to carry out the PC analysis based on the following formula [55]:

$$B_n^m = \frac{4\pi}{2n+1} \frac{|e|^2}{4\pi\epsilon_0} \sum_i \frac{q_i}{r_i^{n+1}} a_0^n \langle r^n \rangle Z_n^m(\theta_i, \phi_i). \quad (8)$$

In our PC analysis, we selected a point-charge shell (≤ 5.45 Å) to describe the CEF environment of Tm^{3+} , including six nearest (2.79 Å) and six next-nearest (4.99 Å) Se^{2-} anions and six nearest Tm^{3+} (4.14 Å) and K^+ (4.48 Å) ions. Although the Se^{2-} ionic shell in the TmSe_6 octahedra is responsible for the primary splitting of the Tm^{3+} manifold, the resulting CEF states are often inaccurate when only six Se^{2-} anions are considered in the CEF environment. This is because the neighboring Tm^{3+} and K^+ ions also contribute significantly to the splitting [45]. The simulated CEF parameters from the selected CEF environment are listed in Table II, while the corresponding eigenvalues and eigenvectors are listed in Table III.

From the PC analysis, we again verified the CEF ground state and the first excited state both to be singlets, dominated by $|J^z = \pm 6\rangle$,

$$|\Psi_0\rangle = 0.51(|6\rangle + |-6\rangle) + 0.35(|3\rangle - |-3\rangle) + 0.48|0\rangle, \quad (9)$$

$$|\Psi_1\rangle = -0.64(|6\rangle - |-6\rangle) - 0.29(|3\rangle + |-3\rangle), \quad (10)$$

TABLE II. CEF parameters B_n^m obtained from PC analysis. The units are in meV.

B_2^0	B_4^0	B_4^3	B_6^0	B_6^3	B_6^6
-1.54×10^{-2}	-7.41×10^{-4}	2.12×10^{-2}	-1.53×10^{-6}	-2.42×10^{-7}	-1.58×10^{-5}

while the energy of $|\Psi_1\rangle$ is ~ 1.17 meV. The results agree with our thermodynamic and neutron scattering measurements well.

In TmMgGaO_4 , the influence of higher CEF levels on low-temperature magnetism below 10 K is negligible due to the large energy gap of approximately 38.4 meV [14]. However, in KTmSe_2 , the three excited states (2.816, 4.798, and 4.837 meV) are somewhat closer to the ground state quasidoublet. This raises concerns about the appropriateness of restricting the analysis to the lower quasidoublet. While this restriction may not be a serious issue for KTmSe_2 , it could be problematic for other rare-earth magnets with weak crystal field splittings. To ensure a comprehensive analysis, we will focus on the effective magnetic Hamiltonian that includes all CEF levels [3,34],

$$\begin{aligned} \hat{H}_{\text{eff}} &= \hat{H}_{\text{CEF}} + \hat{H}_{\text{spin}} \\ &= \sum_{n,m} B_n^m \hat{O}_n^m + \sum_{\langle i,j \rangle} J_x \hat{J}_i^x \hat{J}_j^x + J_y \hat{J}_i^y \hat{J}_j^y + J_z \hat{J}_i^z \hat{J}_j^z. \end{aligned} \quad (11)$$

Due to the apparent Ising anisotropy of Tm^{3+} , it is reasonable to ignore the in-plane spin exchange terms, and then Eq. (11) can be written as

$$\hat{H}_{\text{eff}} = \sum_{n,m} B_n^m \hat{O}_n^m + \sum_{\langle i,j \rangle} J_z \hat{J}_i^z \hat{J}_j^z, \quad (12)$$

where J_z is the nearest out-of-plane exchange parameter and \hat{J}_i^z and \hat{J}_j^z describe the original $J = 6$ operators of the Tm^{3+} moment. By establishing the effective Hamiltonian, we then combine the contributions from all the excited CEF states and the spin exchange interactions. Based on \hat{H}_{eff} , MCPHASE uses the mean-field–random-phase approximation to recalculate the dispersive excitation of the first excited CEF state and find the appropriate parameter value that can accurately describe the present neutron scattering data: $J_z = 0.004$ meV. The calculated result of E - k dispersion shows an excellent agreement with the experimental observation, as shown in Figs. 2(g)–(l) and 3(c).

The exchange parameter value of 0.004 meV simulated from MF-RPA is much smaller than that (0.29 meV) obtained from TFIM, primarily because we focus on the effective total angular momentum $J = 6$ rather than an effective spin $S_{\text{eff}} = 1/2$. Additionally, the antiferromagnetic interaction between Tm^{3+} moments is also consistent with the susceptibility results.

The successful application of PC analysis and MF-RPA calculations to the effective Hamiltonian demonstrates the effectiveness of this method for analyzing CEF excitations in KTmSe_2 . While TFIM can adeptly explain the magnetism by introducing an intrinsic transverse Zeeman term, MF-RPA offers an alternative, complementary approach to explain excitations. The methodology employed in this paper, including the construction and simulation process along with

TABLE III. Calculated eigenvalues and eigenvectors from PC analysis ($\leq 5.45 \text{ \AA}$) on KTmSe_2 .

Eigenvalue (meV)	Eigenvector
0	$0.51(6\rangle + -6\rangle) + 0.354(3\rangle - -3\rangle) + 0.479 0\rangle$
1.171	$-0.643(6\rangle - -6\rangle) - 0.294(3\rangle + -3\rangle)$
2.816	$0.235(5\rangle + -5\rangle) + 0.264(4\rangle - -4\rangle) + 0.342(2\rangle - -2\rangle) + 0.509(1\rangle + -1\rangle)$
2.816	$0.235(5\rangle - -5\rangle) - 0.264(4\rangle + -4\rangle) + 0.342(2\rangle + -2\rangle) - 0.509(1\rangle - -1\rangle)$
4.798	$0.451(6\rangle + -6\rangle) - 0.149(3\rangle - -3\rangle) - 0.74 0\rangle$
4.837	$0.351(5\rangle + -5\rangle) - 0.253(4\rangle - -4\rangle) + 0.449(2\rangle - -2\rangle) - 0.333(1\rangle + -1\rangle)$
4.837	$-0.351(5\rangle - -5\rangle) - 0.253(4\rangle + -4\rangle) - 0.449(2\rangle + -2\rangle) - 0.333(1\rangle - -1\rangle)$
12.394	$0.294(6\rangle - -6\rangle) - 0.643(3\rangle + -3\rangle)$
15.659	$0.434(5\rangle - -5\rangle) - 0.424(4\rangle + -4\rangle) - 0.275(2\rangle + -2\rangle) + 0.236(1\rangle - -1\rangle)$
15.659	$-0.434(5\rangle + -5\rangle) - 0.424(4\rangle - -4\rangle) + 0.275(2\rangle - -2\rangle) + 0.236(1\rangle + -1\rangle)$
15.888	$0.191(6\rangle + -6\rangle) - 0.594(3\rangle - -3\rangle) + 0.472 0\rangle$
16.71	$-0.365(5\rangle + -5\rangle) + 0.432(4\rangle - -4\rangle) + 0.325(2\rangle - -2\rangle) - 0.274(1\rangle + -1\rangle)$
16.71	$0.365(5\rangle - -5\rangle) + 0.432(4\rangle + -4\rangle) - 0.325(2\rangle + -2\rangle) - 0.274(1\rangle - -1\rangle)$

appropriate anisotropic exchange parameters, could be adapted for use with other rare-earth magnets. By providing a versatile approach to analyzing magnetic spectra, this method offers more opportunities to uncover the underlying nature of frustrated rare-earth magnets and explore novel phenomena that may emerge from their unique magnetic characteristics.

V. CONCLUSION

In conclusion, we have successfully synthesized the thulium-based triangular lattice magnet KTmSe_2 . Our comprehensive investigation, including thermodynamic and neutron scattering experiments, has suggested the absence of long-range magnetic order in this compound. Through magnetic susceptibility measurements, we have identified strong Ising-like interactions accompanied by antiferromagnetic correlations. Our inelastic neutron scattering measurements have unveiled a dispersive crystal field excitation branch, which can be accurately described by an effective spin-1/2 model with a transverse field. To further elucidate the CEF states and dispersive excitation, we have employed a point-charge analysis and mean-field-random-phase approximation based on the effective Hamiltonian, taking into account both the CEF interactions and spin exchange interactions. This study

offers a comprehensive understanding of the low-temperature magnetism in KTmSe_2 and provides an effective approach for exploring the intricate magnetic behavior of materials containing $4f$ electrons.

ACKNOWLEDGMENTS

We thank Dr. Martin Rotter for giving precious advice on using MCPHASE. This work was supported by the Key Program of the National Natural Science Foundation of China (Grant No. 12234006), the National Key R&D Program of China (Grant No. 2022YFA1403202), and the Shanghai Municipal Science and Technology Major Project (Grant No. 2019SHZDZX01). H.W. was supported by the China National Postdoctoral Program for Innovative Talents (Grant No. BX2021080), the China Postdoctoral Science Foundation (Grant No. 2021M700860), the Youth Foundation of the National Natural Science Foundation of China (Grant No. 12204108), and the Shanghai Post-doctoral Excellence Program (Grant No. 2021481). G.C. was supported by the Ministry of Science and Technology of China with Grants No. 2021YFA1400300, the National Science Foundation of China with Grant No. 92065203, and the Research Grants Council of Hong Kong with C7012-21GF.

-
- [1] L. Balents, Spin liquids in frustrated magnets, *Nature (London)* **464**, 199 (2010).
- [2] Y. Zhou, K. Kanoda, and T.-K. Ng, Quantum spin liquid states, *Rev. Mod. Phys.* **89**, 025003 (2017).
- [3] Y. Li, G. Chen, W. Tong, L. Pi, J. Liu, Z. Yang, X. Wang, and Q. Zhang, Rare-Earth Triangular Lattice Spin Liquid: A Single-Crystal Study of YbMgGaO_4 , *Phys. Rev. Lett.* **115**, 167203 (2015).
- [4] Y. Shen, Y.-D. Li, H. Wo, Y. Li, S. Shen, B. Pan, Q. Wang, H. C. Walker, P. Steffens, M. Boehm, Y. Hao, D. L. Quintero-Castro, L. W. Harriger, M. D. Frontzek, L. Hao, S. Meng, Q. Zhang, G. Chen, and J. Zhao, Evidence for a spinon fermi surface in a triangular-lattice quantum-spin-liquid candidate, *Nature (London)* **540**, 559 (2016).
- [5] Y. Li, D. Adroja, P. K. Biswas, P. J. Baker, Q. Zhang, J. Liu, A. A. Tsirlin, P. Gegenwart, and Q. Zhang, Muon Spin Relaxation Evidence for the U(1) Quantum Spin-Liquid Ground State in the Triangular Antiferromagnet YbMgGaO_4 , *Phys. Rev. Lett.* **117**, 097201 (2016).
- [6] Y.-D. Li, X. Wang, and G. Chen, Anisotropic spin model of strong spin-orbit-coupled triangular antiferromagnets, *Phys. Rev. B* **94**, 035107 (2016).
- [7] Y.-D. Li, Y.-M. Lu, and G. Chen, Spinon Fermi surface U(1) spin liquid in the spin-orbit-coupled triangular-lattice Mott insulator YbMgGaO_4 , *Phys. Rev. B* **96**, 054445 (2017).
- [8] J. A. M. Paddison, M. Daum, Z. Dun, G. Ehlers, Y. Liu, M. B. Stone, H. Zhou, and M. Mourigal, Continuous excitations of the

- triangular-lattice quantum spin liquid YbMgGaO₄, *Nat. Phys.* **13**, 117 (2017).
- [9] Y. Shen, Y.-D. Li, H. C. Walker, P. Steffens, M. Boehm, X. Zhang, S. Shen, H. Wo, G. Chen, and J. Zhao, Fractionalized excitations in the partially magnetized spin liquid candidate YbMgGaO₄, *Nat. Commun.* **9**, 4138 (2018).
- [10] Y.-D. Li, Y. Shen, Y. Li, J. Zhao, and G. Chen, Effect of spin-orbit coupling on the effective-spin correlation in YbMgGaO₄, *Phys. Rev. B* **97**, 125105 (2018).
- [11] Y.-D. Li and G. Chen, Detecting spin fractionalization in a spinon Fermi surface spin liquid, *Phys. Rev. B* **96**, 075105 (2017).
- [12] C. Liu, Y.-D. Li, and G. Chen, Selective measurements of intertwined multipolar orders: Non-Kramers doublets on a triangular lattice, *Phys. Rev. B* **98**, 045119 (2018).
- [13] Y. Shen, C. Liu, Y. Qin, S. Shen, Y.-D. Li, R. Bewley, A. Schneidewind, G. Chen, and J. Zhao, Intertwined dipolar and multipolar order in the triangular-lattice magnet TmMgGaO₄, *Nat. Commun.* **10**, 4530 (2019).
- [14] Y. Li, S. Bachus, H. Deng, W. Schmidt, H. Thoma, V. Hutanu, Y. Tokiwa, A. A. Tsirlin, and P. Gegenwart, Partial Up-Up-Down Order with the Continuously Distributed Order Parameter in the Triangular Antiferromagnet TmMgGaO₄, *Phys. Rev. X* **10**, 011007 (2020).
- [15] Z. Dun, M. Daum, R. Baral, H. E. Fischer, H. Cao, Y. Liu, M. B. Stone, J. A. Rodriguez-Rivera, E. S. Choi, Q. Huang, H. Zhou, M. Mourigal, and B. A. Frandsen, Neutron scattering investigation of proposed Kosterlitz-Thouless transitions in the triangular-lattice Ising antiferromagnet TmMgGaO₄, *Phys. Rev. B* **103**, 064424 (2021).
- [16] Y. Qin, Y. Shen, C. Liu, H. Wo, Y. Gao, Y. Feng, X. Zhang, G. Ding, Y. Gu, Q. Wang, S. Shen, H. C. Walker, R. Bewley, J. Xu, M. Boehm, P. Steffens, S. Ohira-Kawamura, N. Murai, A. Schneidewind, X. Tong *et al.*, Field-tuned quantum effects in a triangular-lattice Ising magnet, *Sci. Bull.* **67**, 38 (2022).
- [17] G. Chen, Intrinsic transverse field in frustrated quantum Ising magnets: Physical origin and quantum effects, *Phys. Rev. Res.* **1**, 033141 (2019).
- [18] C. Liu, C.-J. Huang, and G. Chen, Intrinsic quantum Ising model on a triangular lattice magnet TmMgGaO₄, *Phys. Rev. Res.* **2**, 043013 (2020).
- [19] J. G. Rau and M. J. P. Gingras, Frustration and anisotropic exchange in ytterbium magnets with edge-shared octahedra, *Phys. Rev. B* **98**, 054408 (2018).
- [20] C. Liu, F.-Y. Li, and G. Chen, Upper branch magnetism in quantum magnets: Collapses of excited levels and emergent selection rules, *Phys. Rev. B* **99**, 224407 (2019).
- [21] S. Voleti, F. D. Wandler, and A. Paramekanti, Impact of gapped spin-orbit excitons on low energy pseudospin exchange interactions, [arXiv:2303.04169](https://arxiv.org/abs/2303.04169).
- [22] L. S. Wu, S. E. Nikitin, M. Brando, L. Vasylechko, G. Ehlers, M. Frontzek, A. T. Savici, G. Sala, A. D. Christianson, M. D. Lumsden, and A. Podlesnyak, Antiferromagnetic ordering and dipolar interactions of YbAlO₃, *Phys. Rev. B* **99**, 195117 (2019).
- [23] T. T. A. Lummen, I. P. Handayani, M. C. Donker, D. Fausti, G. Dhalenne, P. Berthet, A. Revcolevschi, and P. H. M. van Loosdrecht, Phonon and crystal field excitations in geometrically frustrated rare earth titanates, *Phys. Rev. B* **77**, 214310 (2008).
- [24] M. Mączka, M. L. Sanjuan, A. F. Fuentes, K. Hermanowicz, and J. Hanuza, Temperature-dependent Raman study of the spin-liquid pyrochlore Tb₂Ti₂O₇, *Phys. Rev. B* **78**, 134420 (2008).
- [25] M. Ruminy, E. Pomjakushina, K. Iida, K. Kamazawa, D. T. Adroja, U. Stuhr, and T. Fennell, Crystal-field parameters of the rare-earth pyrochlores R₂Ti₂O₇ (R = Tb, Dy, and Ho), *Phys. Rev. B* **94**, 024430 (2016).
- [26] K. Iwasa, Neutron scattering studies on 4f²-electron multipoles in Pr-based systems, *J. Phys. Soc. Jpn.* **88**, 081005 (2019).
- [27] C.-K. Li and G. Chen, Universal excitonic superexchange in spin-orbit-coupled Mott insulators, *Europhys. Lett.* **139**, 56001 (2022).
- [28] W. Liu, Z. Zhang, J. Ji, Y. Liu, J. Li, X. Wang, H. Lei, G. Chen, and Q. Zhang, Rare-earth chalcogenides: A large family of triangular lattice spin liquid candidates, *Chin. Phys. Lett.* **35**, 117501 (2018).
- [29] M. M. Bordelon, E. Kenney, C. Liu, T. Hogan, L. Posthuma, M. Kavand, Y. Lyu, M. Sherwin, N. P. Butch, C. Brown, M. J. Graf, L. Balents, and S. D. Wilson, Field-tunable quantum disordered ground state in the triangular-lattice antiferromagnet NaYbO₂, *Nat. Phys.* **15**, 1058 (2019).
- [30] K. M. Ranjith, D. Dmytriieva, S. Khim, J. Sichelschmidt, S. Luther, D. Ehlers, H. Yasuoka, J. Wosnitza, A. A. Tsirlin, H. Kühne, and M. Baenitz, Field-induced instability of the quantum spin liquid ground state in the $J_{\text{eff}} = \frac{1}{2}$ triangular-lattice compound NaYbO₂, *Phys. Rev. B* **99**, 180401(R) (2019).
- [31] L. Ding, P. Manuel, S. Bachus, F. Grüßler, P. Gegenwart, J. Singleton, R. D. Johnson, H. C. Walker, D. T. Adroja, A. D. Hillier, and A. A. Tsirlin, Gapless spin-liquid state in the structurally disorder-free triangular antiferromagnet NaYbO₂, *Phys. Rev. B* **100**, 144432 (2019).
- [32] R. Sarkar, P. Schlender, V. Grinenko, E. Haeussler, P. J. Baker, T. Doert, and H.-H. Klauss, Quantum spin liquid ground state in the disorder free triangular lattice NaYbS₂, *Phys. Rev. B* **100**, 241116(R) (2019).
- [33] K. M. Ranjith, S. Luther, T. Reimann, B. Schmidt, P. Schlender, J. Sichelschmidt, H. Yasuoka, A. M. Strydom, Y. Skourski, J. Wosnitza, H. Kühne, T. Doert, and M. Baenitz, Anisotropic field-induced ordering in the triangular-lattice quantum spin liquid NaYbSe₂, *Phys. Rev. B* **100**, 224417 (2019).
- [34] Z. Zhang, J. Li, W. Liu, Z. Zhang, J. Ji, F. Jin, R. Chen, J. Wang, X. Wang, J. Ma, and Q. Zhang, Effective magnetic Hamiltonian at finite temperatures for rare-earth chalcogenides, *Phys. Rev. B* **103**, 184419 (2021).
- [35] P.-L. Dai, G. Zhang, Y. Xie, C. Duan, Y. Gao, Z. Zhu, E. Feng, Z. Tao, C.-L. Huang, H. Cao, A. Podlesnyak, G. E. Granroth, M. S. Everett, J. C. Neufeind, D. Voneshen, S. Wang, G. Tan, E. Morosan, X. Wang, H.-Q. Lin *et al.*, Spinon Fermi Surface Spin Liquid in a Triangular Lattice Antiferromagnet NaYbSe₂, *Phys. Rev. X* **11**, 021044 (2021).
- [36] A. O. Scheie, E. A. Ghioldi, J. Xing, J. A. M. Paddison, N. E. Sherman, M. Dupont, L. D. Sanjeeva, S. Lee, A. J. Woods, D. Abernathy, D. M. Pajerowski, T. J. Williams, S.-S. Zhang, L. O. Manuel, A. E. Trumper, C. D. Pemmaraju, A. S. Sefat, D. S. Parker, T. P. Devereaux, R. Movshovich *et al.*, Witnessing quantum criticality and entanglement in the triangular antiferromagnet KYbSe₂, [arXiv:2109.11527](https://arxiv.org/abs/2109.11527).
- [37] A. O. Scheie, Y. Kamiya, H. Zhang, S. Lee, A. J. Woods, M. G. Gonzalez, B. Bernu, J. Xing, Q. Huang, Q. M. Zhang, J. Ma, E. S. Choi, D. M. Pajerowski, H. Zhou, A. S. Sefat, L. Messio,

- R. Movshovich, C. D. Batista, and D. A. Tennant, Non-linear magnons and exchange Hamiltonians of delafossite proximate quantum spin liquids, [arXiv:2207.14785](https://arxiv.org/abs/2207.14785).
- [38] J. Xing, L. D. Sanjeewa, J. Kim, G. R. Stewart, A. Podlesnyak, and A. S. Sefat, Field-induced magnetic transition and spin fluctuations in the quantum spin-liquid candidate CsYbSe₂, *Phys. Rev. B* **100**, 220407(R) (2019).
- [39] J. Xing, L. D. Sanjeewa, J. Kim, W. R. Meier, A. F. May, Q. Zheng, R. Custelcean, G. R. Stewart, and A. S. Sefat, Synthesis, magnetization, and heat capacity of triangular lattice materials NaErSe₂ and KErSe₂, *Phys. Rev. Mater.* **3**, 114413 (2019).
- [40] J. Xing, K. M. Taddei, L. D. Sanjeewa, R. S. Fishman, M. Daum, M. Mourigal, C. dela Cruz, and A. S. Sefat, Stripe antiferromagnetic ground state of the ideal triangular lattice compound KErSe₂, *Phys. Rev. B* **103**, 144413 (2021).
- [41] G. Ding, H. Wo, R. L. Luo, Y. Gu, Y. Gu, R. Bewley, G. Chen, and J. Zhao, Stripe order and spin dynamics in the triangular-lattice antiferromagnet KErSe₂: A single-crystal study with a theoretical description, *Phys. Rev. B* **107**, L100411 (2023).
- [42] G. Bastien, B. Rubrecht, E. Haeussler, P. Schlender, Z. Zangeneh, S. Avdoshenko, R. Sarkar, A. Alfonsov, S. Luther, Y. A. Onykiienko, H. C. Walker, H. Kühne, V. Grinenko, Z. Guguchia, V. Kataev, H. H. Klauss, L. Hozoi, J. van den Brink, D. S. Inosov, B. Büchner *et al.*, Long-range magnetic order in the $S = 1/2$ triangular lattice antiferromagnet KCeS₂, *SciPost Phys.* **9**, 041 (2020).
- [43] A. A. Kulbakov, S. M. Avdoshenko, I. Puente-Orench, M. Deeb, M. Doerr, P. Schlender, T. Doert, and D. S. Inosov, Stripe- $\gamma\delta$ magnetic order in the triangular-lattice antiferromagnet KCeS₂, *J. Phys.: Condens. Matter* **33**, 425802 (2021).
- [44] S. M. Avdoshenko, A. A. Kulbakov, E. Häußler, P. Schlender, T. Doert, J. Ollivier, and D. S. Inosov, Spin-wave dynamics in the KCeS₂ delafossite: A theoretical description of powder inelastic neutron-scattering data, *Phys. Rev. B* **106**, 214431 (2022).
- [45] M. M. Bordelon, C. Liu, L. Posthuma, P. M. Sarte, N. P. Butch, D. M. Pajerowski, A. Banerjee, L. Balents, and S. D. Wilson, Spin excitations in the frustrated triangular lattice antiferromagnet NaYbO₂, *Phys. Rev. B* **101**, 224427 (2020).
- [46] M. Baenitz, P. Schlender, J. Sichelschmidt, Y. A. Onykiienko, Z. Zangeneh, K. M. Ranjith, R. Sarkar, L. Hozoi, H. C. Walker, J.-C. Orain, H. Yasuoka, J. van den Brink, H. H. Klauss, D. S. Inosov, and T. Doert, NaYbS₂: A planar spin-1/2 triangular-lattice magnet and putative spin liquid, *Phys. Rev. B* **98**, 220409(R) (2018).
- [47] Z. Zhang, X. Ma, J. Li, G. Wang, D. T. Adroja, T. P. Perring, W. Liu, F. Jin, J. Ji, Y. Wang, Y. Kamiya, X. Wang, J. Ma, and Q. Zhang, Crystalline electric field excitations in the quantum spin liquid candidate NaYbSe₂, *Phys. Rev. B* **103**, 035144 (2021).
- [48] C. A. Pocs, P. E. Siegfried, J. Xing, A. S. Sefat, M. Hermele, B. Normand, and M. Lee, Systematic extraction of crystal electric-field effects and quantum magnetic model parameters in triangular rare-earth magnets, *Phys. Rev. Res.* **3**, 043202 (2021).
- [49] S. Gao, F. Xiao, K. Kamazawa, K. Ikeuchi, D. Biner, K. W. Krämer, C. Rüegg, and T.-h. Arima, Crystal electric field excitations in the quantum spin liquid candidate NaErS₂, *Phys. Rev. B* **102**, 024424 (2020).
- [50] A. Scheie, V. O. Garlea, L. D. Sanjeewa, J. Xing, and A. S. Sefat, Crystal-field Hamiltonian and anisotropy in KErSe₂ and CsErSe₂, *Phys. Rev. B* **101**, 144432 (2020).
- [51] M. M. Bordelon, X. Wang, D. M. Pajerowski, A. Banerjee, M. Sherwin, C. M. Brown, M. S. Eldeeb, T. Petersen, L. Hozoi, U. K. Röbber, M. Mourigal, and S. D. Wilson, Magnetic properties and signatures of moment ordering in the triangular lattice antiferromagnet KCeO₂, *Phys. Rev. B* **104**, 094421 (2021).
- [52] B. R. Ortiz, M. M. Bordelon, P. Bhattacharyya, G. Pokharel, P. M. Sarte, L. Posthuma, T. Petersen, M. S. Eldeeb, G. E. Granroth, C. R. Dela Cruz, S. Calder, D. L. Abernathy, L. Hozoi, and S. D. Wilson, Electronic and structural properties of RbCeX₂ (X₂: O₂, S₂, SeS, Se₂, TeSe, Te₂), *Phys. Rev. Mater.* **6**, 084402 (2022).
- [53] J. Rodríguez-Carvajal, Recent advances in magnetic structure determination by neutron powder diffraction, *Phys. B* **192**, 55 (1993).
- [54] K. W. H. Stevens, Matrix elements and operator equivalents connected with the magnetic properties of rare earth ions, *Proc. Phys. Soc. London Sect. A* **65**, 209 (1952).
- [55] M. Rotter, Using *McPhase* to calculate magnetic phase diagrams of rare earth compounds, *J. Magn. Magn. Mater.* **272-276**, E481 (2004).